Birck and NCN Publications   Birck Nanotechnology Center

1-2010

On Landauer versus Boltzmann and full band versus effective mass evaluation of thermoelectric transport coefficients

Changwook Jeong
Electrical and Computer Engineering, Purdue University, jeongc@purdue.edu

Raseong Kim
Purdue University - Main Campus

Mathieu Luisier
Purdue University - Main Campus, mluisier@purdue.edu

Supriyo Datta
Birck Nanotechnology Center and Purdue University, datta@purdue.edu

Mark S. Lundstrom
School of Electrical and Computer Engineering, Birck Nanotechnology Center, Purdue University, lundstro@purdue.edu

Follow this and additional works at: http://docs.lib.purdue.edu/nanopub

Part of the Nanoscience and Nanotechnology Commons

On Landauer versus Boltzmann and full band versus effective mass evaluation of thermoelectric transport coefficients

Changwook Jeong,[a)] Raseong Kim, Mathieu Luisier, Supriyo Datta, and Mark Lundstrom
Network for Computational Nanotechnology, Birck Nanotechnology Center, Purdue University, West Lafayette, Indiana 47907, USA

Using a full band description of electronic bandstructure, the Landauer approach to diffusive transport is mathematically related to the solution of the Boltzmann transport equation, and expressions for the thermoelectric parameters in both formalisms are presented. Quantum mechanical and semiclassical techniques to obtain from a full description of the bandstructure, $E(k)$, the density of modes in the Landauer approach or the transport distribution in the Boltzmann solution are compared and thermoelectric transport coefficients are evaluated. Several example calculations for representative bulk materials are presented and the full band results are related to the more common effective mass formalism. Finally, given a full $E(k)$ for a crystal, a procedure to extract an accurate, effective mass level description is presented. © *2010 American Institute of Physics*. [doi:10.1063/1.3291120]

I. INTRODUCTION

Much experimental and theoretical effort has been directed at improving the thermoelectric (TE) figure of merit, $ZT = S^2GT/K$, where T is the temperature, S is the Seebeck coefficient, G is the electrical conductance, and K is the thermal conductance, which is the sum of the electronic contribution, K_e, and the lattice thermal conductance, K_l. Careful tradeoffs are needed to obtain high ZT. Recent experimental reports of high ZT[1–8] are attributed to suppressing the lattice thermal conductivity, and now the question of whether the electronic performance can be enhanced is being asked.[9–11] New materials,[1,12–15] new structures (e.g., nanowires,[16–26] quantum wells,[2,27,28] superlattices,[10,11,17,29–36] and nanocomposites[3,4,37–39]), and strain engineering,[29,40–42] which has been so successful for enhancing the electronic performance of nanotransistors, are all being explored. To address these opportunities, TE coefficients must be related to an accurate description of the electronic structure of the material.

TE parameters are usually evaluated by solving the Boltzmann transport equation (BTE).[43] For low temperature TEs in mesoscopic structures, the Landauer approach is commonly used.[44,45] The Landauer approach applies to high temperature diffusive samples as well, and it provides an alternative formulation that can be insightful.[46] One objectives for this paper are to discuss the mathematical relation between the Landauer and Boltzmann approaches when using a full description of the electronic bandstructure and to relate the full band calculations to effective mass level descriptions

In both the Landauer and Boltzmann approaches the TE parameters are related to the electronic structure of the material. The effective mass approach is widely-used to analyze experiments and to design devices. For more complex materials, full band treatments (*ab initio* or empirical tight binding) have been used.[12,47–56] It is still not clear, however, exactly how full band treatments relate to effective mass level treatments—especially for complex bandstructures. Another objective of this paper is to discuss the evaluation of TE parameters from a full band perspective and to show that the results are easily related to an effective mass level description.

The paper is organized as follows. In Sec. II, we present a brief summary of the Landauer formalism and relate it to the more common approach that begins with the BTE. We also present two methods for evaluating the transport distribution in the Landauer approach from a full band description of the electronic structure. In Sec. III, tight binding simulation results are presented for the conduction bands (CBs) and valence bands (VBs) of germanium (Ge), gallium arsenide (GaAs), and bismuth telluride (Bi_2Te_3). The results are discussed within the Landauer framework in Sec. IV, as is the relation of the rigorous approach to the effective mass approach. Our conclusions are summarized in Sec. V.

II. APPROACH

The Landauer formalism in the linear response regime gives the electrical conductance, Seebeck coefficient, and the thermal conductance for zero electric current as[57,58]

$$G = (2q^2/h)I_0 \quad [1/\Omega], \tag{1}$$

$$S = [k_B/(-q)]\frac{I_1}{I_0} \quad [V/K], \tag{2}$$

$$K_e = (T_L 2k_B^2/h)\{I_2 - I_1^2/I_0\} \quad [W/K], \tag{3}$$

where

$$I_j = \int_{-\infty}^{+\infty} \left(\frac{E - E_F}{k_B T_L}\right)^j \bar{T}(E)\left(-\frac{\partial f_0}{\partial E}\right)dE, \tag{4}$$

with

a)Electronic mail: jeong.changwook@gmail.com.

$$\bar{T}(E) = T(E)M(E), \quad (5)$$

being the transmission,[45] and $M(E)$ the density of modes (DOM).[59] For a conductor of length, L, and mean-free-path for backscattering, $\langle\langle\lambda(E)\rangle\rangle$,

$$T(E) = \langle\langle\lambda(E)\rangle\rangle/L \quad (6)$$

in the diffusive limit.[59] For some common scattering mechanisms, $\langle\langle\lambda(E)\rangle\rangle$ can be expressed in power law form as $\langle\langle\lambda(E)\rangle\rangle = \lambda_0(E/k_BT)^r$, where λ_0 is a constant, E is the kinetic energy, and r is a characteristic exponent describing a specific scattering process.

TE transport coefficients are more commonly obtained by solving the Boltzmann equation in the relaxation time approximation and expressed in terms of an integral like Eq. (4) with the transmission replaced by the so-called transport distribution according to[46]

$$\Sigma(E) = \frac{L^2}{h}M(E)T(E) = \frac{L}{h}M(E)\langle\langle\lambda\rangle\rangle. \quad (7)$$

A solution of the Boltzmann equation gives[43]

$$\Sigma(E) = \sum_{\vec{k}}(v_x^2\tau)\delta(E - E_k), \quad (8)$$

where τ is the momentum relaxation time. Equation (7) relates the solution of the Boltzmann equation in the relaxation time approximation to the Landauer formalism.

By making the definition

$$\langle|v_x|\rangle \equiv \frac{\sum_{\vec{k}}|v_x|\delta(E - E_k)}{\sum_{\vec{k}}\delta(E - E_k)}, \quad (9)$$

Eq. (8) can be expressed as

$$\sum(E) = \frac{\langle v_x^2\tau\rangle}{\langle|v_x|\rangle}\langle|v_x|\rangle D(E) = \frac{\langle v_x^2\tau\rangle}{\langle|v_x|\rangle}\sum_k|v_x|\delta(E - E_k), \quad (10)$$

where $D(E) = \sum_k\delta(E - E_k)$ is the density of states (DOS).

Finally, according to Eq. (7), we find

$$M(E) = \frac{h}{2L}\sum_k|v_x|\delta(E - E_k) \quad (11)$$

and

$$\langle\langle\lambda(E)\rangle\rangle = 2\frac{\langle v_x^2\tau\rangle}{\langle|v_x|\rangle}. \quad (12)$$

Equation (11) is a well-known result that relates the DOM in the Landauer formalism to the bandstructure.[45,59] Equation (12) is a new results that define an appropriately defined mean-free-path (the mean-free-path for backscattering) so that the Landauer results agree with the Boltzmann equation in the relaxation time approximation. Assuming isotropic energy bands, Eq. (12) can be evaluated in one-dimension (1D), two-dimensions (2D), and three-dimensions (3D) to find

$$\langle\langle\lambda(E)\rangle\rangle = 2v(E)\tau(E) \quad \text{(1D)}, \quad (13a)$$

$$\langle\langle\lambda(E)\rangle\rangle = (\pi/2)v(E)\tau(E) \quad \text{(2D)}, \quad (13b)$$

$$\langle\langle\lambda(E)\rangle\rangle = (4/3)v(E)\tau(E) \quad \text{(3D)}. \quad (13c)$$

In practice, a constant scattering time is often assumed for the Boltzmann equation, but this is hard to justify. In the Landauer approach, a constant mean-free-path simplifies calculations and can be justified in 3D for parabolic bands when the scattering rate is proportional to the DOS.

The discussion above shows that $M(E)$ is essentially the carrier velocity times the DOS. If we consider a single parabolic CB, $E = \hbar^2k^2/2m^*$, then $M(E)$ for 3D is

$$M(E) = A\frac{m_{DOM}^*}{2\pi\hbar^2}E, \quad (14)$$

where the DOM effective mass (m_{DOM}^*) is just m^* for a single, spherical band. (Results for 1D and 2D are given in Ref. 46) For ellipsoidal energy bands, Eq. (11) can be evaluated for each equivalent ellipsoid to find $m_{DOM}^* = \sqrt{m_y^*m_z^*}$ with the direction of current flow being along the x-direction. This example shows that $M(E)$ is related to the DOS in the 2D plane transverse to the transport direction. The contributions for each equivalent ellipsoid are then summed. For the CB of silicon, the result is $m_{DOM}^* = 2m_t^* + 4\sqrt{m_t^*m_1^*}$ which is $2.04m_0$. Recall that the DOS effective mass is $m_{DOS}^* = 6^{2/3}(m_1m_t^2)^{1/3} = 1.06m_0$. This example shows that the DOM and DOS effective masses can be quite different. The DOS and the DOM effective mass in the Landuaer approach are analogous to the DOS and the conductivity effective mass in the Boltzmann approach. Finally, for nonparabolic bands with Kane's dispersion relation,[60] $E(1 + \alpha E) = \hbar^2k^2/2m^*$, $M(E)$ for 3D becomes

$$M(E) = A\frac{m^*}{2\pi\hbar^2}E(1 + \alpha E), \quad (15)$$

where α is the nonparabolicity parameter. These analytical results will be our reference against which we compare the numerical results to be presented later.

Two procedures are available to numerically evaluate $M(E)$. First, $M(E)$ can be calculated by counting bands for a given bandstructure, because we can express Eq. (11) as[59,61]

$$M(E) = \sum_{k_\perp}\Theta(E - E_{k_\perp}), \quad (16)$$

where Θ is the unit step function and $k_\perp$ refers to k states perpendicular to the transport direction (i.e., transverse modes). Equation (16) is simply a count of the bands that cross the energy of interest and provides a computationally simple way to obtain $M(E)$ from a given $E(k)$. Similar expressions have been used to numerically evaluate the DOM for phonon transport from a given dispersion relations.[62] A MATLAB® script that implements this calculation for Ge is available.[63]

An alternative to counting the number of available bands at a given energy consists of calculating the transmission coefficient through a given structure as function of the injection energy. In the nonequilibrium Green's function formalism,[59] $\bar{T}(E)$ is

$$\bar{T}(E) = Tr(\Gamma_1 G \Gamma_2 G^\dagger), \tag{17}$$

where G is the retarded Green's function and

$$\Gamma_{1,2} = \mathbf{i}\left(\Sigma_{1,2} - \Sigma_{1,2}^\dagger\right), \tag{18}$$

where $\Sigma_{1,2}$ are the contact self-energies. This approach works for bulk TEs, but it also allows us to obtain the TE parameters for quantum-engineered structures for which the electronic structure may be very different from the bulk.

For our calculations, we have developed a multidimensional quantum transport simulator based on different flavors of the nearest-neighbor tight-binding model. It solves Schrödinger equation in the wave function formalism, which in the ballistic limit is equivalent to the nonequilibrium Green's function (NEGF), but computationally much more efficient.[64] To obtain the bulk transmission coefficient $\bar{T}(E)$, a small device structure composed of two to three unit cells is constructed, two semi-infinite contacts are attached to both ends of the simulation domain, and electrons and holes are injected and collected from these contacts. This procedure is repeated for different energies and wave vectors so that the entire Brillouin zone of the considered semiconductor material is spanned. We integrate the resulting transmission coefficient over its momentum-dependence at a given energy to evaluate $\bar{T}(E)$.

To evaluate $M(E)$ beyond the effective mass approximation, an accurate description of the electronic structure is needed. Materials like Si, Ge, or GaAs have been parameterized in the nearest-neighbor tight-binding (TB) model by several groups[65–67] with different levels of approximation [e.g., sp^3s^* (Ref. 68) and $sp^3d^5s^*$ (Ref. 67) models] for many years. More exotic materials like Bi_2Te_3 have been parameterized.[47,48] A comparison with energy bands obtained from density functional theory shows that a nearest-neighbor $sp^3d^5s^*$ tight-binding approach with spin-orbit coupling is required to capture the essential characteristics of the Bi_2Te_3 bandstructure.[48] Hence, we have extended our quantum transport simulator described above to include the rhombohedral crystal lattice and to calculate transmission coefficients through such structures.

III. RESULTS

In this section, we illustrate the techniques discussed in Sec. II and show how full band calculations are related to effective mass calculations. A few materials that are good illustrations (not necessarily good TE materials) are compared: (a) Ge to compare three approaches to compute the DOM-counting bands, NEGF-TB model, effective mass approximation (EMA)—which should all agree rather well since the Ge CBs are nearly parabolic, (b) Ge VB to see if we can use an effective mass description for VB, (c) GaAs to illustrate the effect of nonparabolicity, and (d) Bi_2Te_3 because it is commonly used TE with a more complex bandstructure.
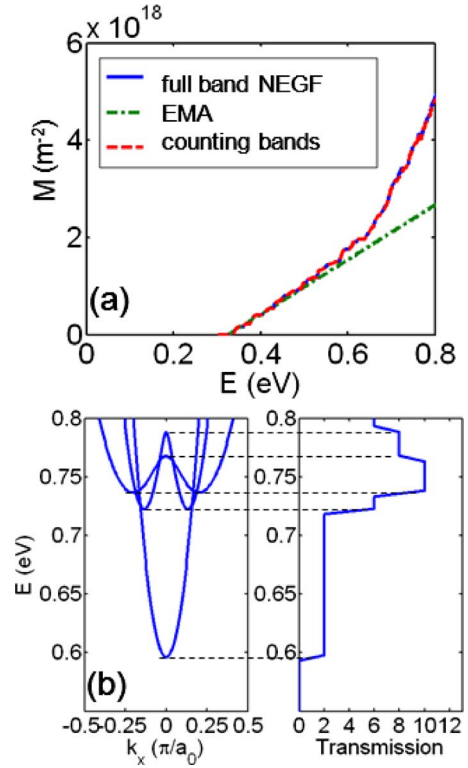

FIG. 1. (Color online) (a) Comparison of the DOMs, $M(E)$, computed by three different approaches for Germanium (Ge): NEGF-TB model, EMA, and counting bands. The $M(E)$ from counting bands (dashed line) is on top of $M(E)$ from the NEFG-TB model. (b) Illustration of bands counting method for specific dispersion relation for Ge. Dotted line is guide to eye.

Figure 1 shows the DOM, $M(E)$ for the Ge CB as computed by three different approaches. Counting bands gives exactly the same $M(E)$ obtained by NEGF-TB model. As shown in Fig. 1, the EMA expression for $M(E)$ [Eq. (14)] provides a good fit to the full band calculation near the CB edge. Full band calculations of the DOS, $D(E)$ and $M(E)$ for Ge, GaAs, and Bi_2Te_3 are shown in Fig. 2. Around the band edge, the linear DOM $M(E)$ versus energy expected from Eq. (14) is observed for all materials considered—even for the highly warped VB. In the bulk, $M(E)$ varies linearly with E because both $D(E)$ and $\upsilon(E)$ are proportional to $\sqrt{E}$. A linear behavior of the "transport distribution" $\Sigma(E)$ versus E has previously been observed,[49] but the transport distribution varies as $D(E)$ times $\upsilon^2(E)$, so it is not expected to be exactly linear when the relaxation time, τ, is assumed to be constant.

To show the relation between full band calculation and the EMA, a "DOM" effective mass (m^*_{DOM}) was extracted from the numerically evaluated $M(E)$ using Eq. (14) and compared to the analytical m^*_{DOM} with number of valleys and transport direction being accounted for. The results are listed in Table I. The discrepancy is no larger than 10% for CB, while it is about a factor of 2 for VB. As shown in Fig. 3 for the CB of GaAs, a better fit can be obtained when nonparabolicity is accounted for, and the discrepancy between extracted m^*_{DOM} and analytic one reduced from 10% to 2%. As listed in Table I and discussed in Sec. II, the DOS effective masses are clearly different from the DOM effective masses-except for GaAs, where the Gamma valley is the CB minimum. Finally, note that although there is no simple relation
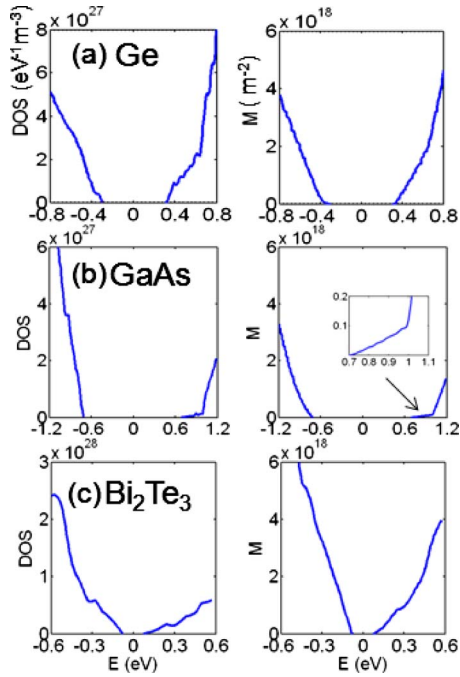
FIG. 2. (Color online) Full band calculations of the DOS and the DOM $M(E)$ for Ge, GaAs, and Bi$_2$Te$_3$. The midgap is located at $E = 0$. The inset in (b) shows $M(E)$ near the CB edge for GaAs.

between the light and heavy hole effective masses and the numerically extracted m^*_{DOM} for the VB, a constant m^*_{DOM} provides a good fit to $\bar{T}(E)$.

IV. DISCUSSION

In this section, TE properties will be evaluated and interpreted within the Landauer framework. Figure 4 compares calculated Seebeck coefficients (S) using Eq. (2) to experiments. The results are plotted versus reduced Fermi level

TABLE I. Analytic DOM and full band NEGF-TB simulation. For comparison, DOS effective masses (m^*_{DOS}) are also listed. The transport direction is along the x direction. The electron (m^e) and hole effective masses ($m^{\text{lh}}, m^{\text{hh}}$) in the device coordinate (x, y, z) are used for analytic effective mass calculations and are given in units of the free electron mass. The "heavy-hole" effective masses (Ge: 0.35 and GaAs: 0.51) assume spherical symmetry (Refs. 74 and 75). The extracted heavy-hole effective mass for Ge and GaAs has a strong anisotropy (Ge: 0.17 [100], 0.37 [110], 0.53 [111], and GaAs: 0.38 [100], 0.66 [110], 0.84 [111]). CB denotes conduction band and VB denotes valence band. The top three rows are for the CBs and generally show good agreement between analytic and numerically extracted values. The bottom three rows for VB generally show a much larger discrepancy. The two columns at the right show that analytic and numerically extracted DOS effective masses generally agree reasonably well, but the DOS effective masses are typically much lower than the DOM effective masses.

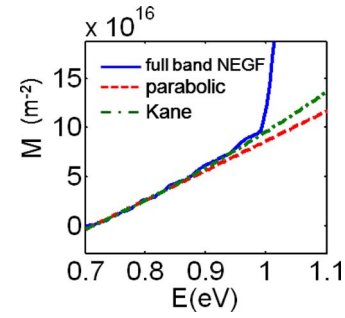| Material	m^*_{DOM}		m^*_{DOS}	
	Analytic	Extracted	Analytic	Extracted
Ge CB	$4\sqrt{m^e_{yy}m^e_{zz}} = 1.18$	1.24	0.56	0.51
GaAs CB	$m_{yy} = 0.066$	0.073	0.066	0.063
Bi$_2$Te$_3$ CB	$2\sqrt{m^e_{xx}m^e_{zz}} + 4\sqrt{m^e_{yy}m^e_{zz}} = 1.18$	1.17	0.23	0.28
Ge VB	$m^{\text{lh}}_{yy} + m^{\text{hh}}_{yy} = 0.37$	1.63	0.35	0.32
GaAs VB	$m^{\text{lh}}_{yy} + m^{\text{hh}}_{yy} = 0.59$	0.97	0.52	0.39
Bi$_2$Te$_3$ VB	$2\sqrt{m^h_{xx}m^h_{zz}} + 4\sqrt{m^h_{yy}m^h_{zz}} = 1.39$	3.53	0.36	0.41

FIG. 3. (Color online) Comparison of fitting based on parabolic dispersion relation with fitting based on Kane dispersion relation. Nonparabolicity parameter α used or GaAs is 0.64 (Ref. 71). Above 1 eV, L valleys contribute to the DOM in addition to Γ valley.

$[\eta_F = (E_F - E_C)/k_B T]$, and we assume that the scattering rate $(1/\tau)$ is proportional to the DOS, i.e., phonon scattering is dominant,[69] which is equivalent to a constant mean-free-path, λ_0. The Seebeck coefficient [Eq. (2)] is independent of λ_0 The results clearly demonstrate that S is nearly independent of electronic band structure (i.e., of m^*_{DOM}). In the effective mass approximation, the Seebeck coefficient in 3D is $S_{3D} = -(k_B/q)[(r+2)\mathfrak{F}_{r+1}(\eta_F)/\mathfrak{F}_r(\eta_F) - \eta_F]$, which depends only on the location of the Fermi level and on r, where r is the characteristic exponent that describes scattering. The Seebeck coefficient depends weakly on electronic structure but more strongly on scattering. Ioffe, for example, pointed out the possibility of making use of ionized impurity scattering ($r = 2$) to improve S.[70]

The constant mean-free-path was adjusted to give the best match to experimental data for electrical conductivity (σ) with its corresponding S. This approach is essentially the same as the common approach in which the unknown relaxation time, τ, is treated as a constant,[40,48,49,71] which actually turned out to be good approximation even for systems with crystal anisotropy.[49,71] With the best fit λ_0, the power factor ($PF = S^2 G$) and electronic thermal conductivity (κ_e) were then evaluated using Eqs. (1)–(3). The TE figure of merit, ZT was computed at 300 K using calculated values of PF and κ_e and the experimentally determined the lattice thermal conductivity, κ_l.[69] Figure 5 shows well-fitted results for Bi$_2$Te$_3$ with $\lambda_0 = 18, 4$ nm for CB and VB, respectively. Figure 6
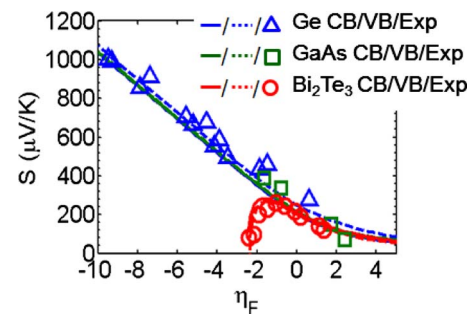

FIG. 4. (Color online) Calculated Seebeck coefficients (S) using Eq. (2) and experiments (Refs. 67 and 72–74) as a function of reduced Fermi level ($\eta_F = (E_F - E_C)/k_B T$) We assumed that scattering rate $(1/\tau)$ is proportional to the DOS, i.e., phonon scattering is dominant.(Ref. 67) The reduction in S around $\eta_F = -2$ for Bi$_2$Te$_3$ is attributed to the bipolar conduction due to its relatively small bandgap (0.162 eV).
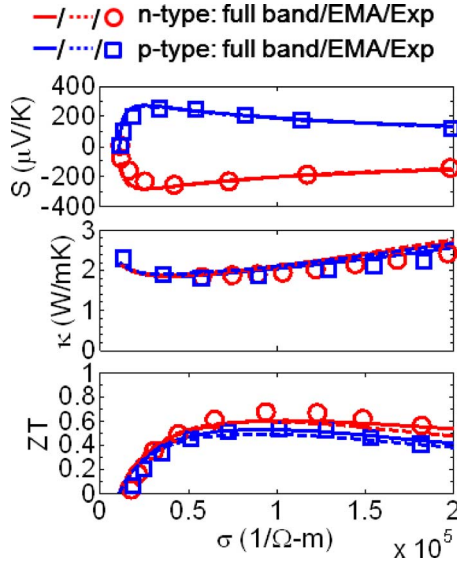
FIG. 5. (Color online) Comparison of the simulated and experimentally measured S, G, and κ for Bi_2Te_3 assuming a constant mean-free-path, λ_0 =18, 4 nm for CBs and VBs. Thermal conductivity is the sum of the electronic and lattice thermal conductivity. Used parameters are listed in Table II.

compares the calculated *PF* and *ZT* versus Fermi level to experiments for Ge, GaAs, and Bi_2Te_3. Calculated results agree well with experiments. (The parameters used in these calculations are summarized in Table II.) These results show that the Landauer approach gives essentially the same accuracy as the BTE approach (although the use of a constant mean-free-path is easier to justify than the use of a constant relaxation time). The Landauer approach has the benefit of being readily extendable to ballistic (e.g., thermionic) and to quantum-engineered structures.

We now consider the effective mass level treatment of this problem. To calculate TE coefficients and analyze measured TE data within the EMA, two effective masses are
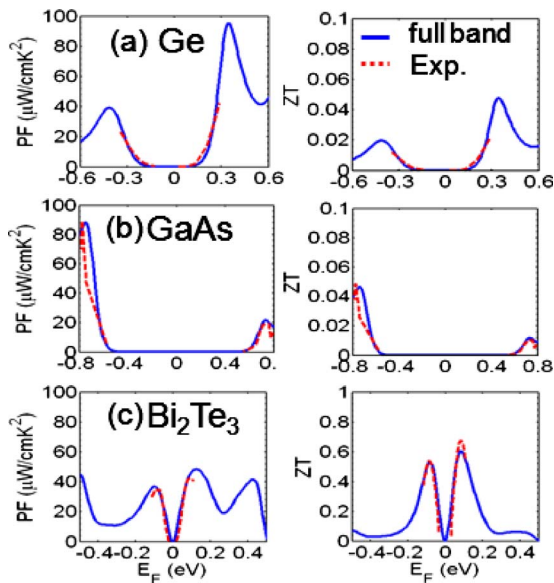

FIG. 6. (Color online) Calculated and measured *PF* and *ZT* as function of the Fermi level. Used parameters are listed in Table II.

TABLE II. Summary of parameters used in Fig. 6: fitted λ_0(nm) parameters, experimental lattice thermal conductivity κ_l(Wm^{-1} K^{-1}). In the power law form of the mean free path, $\langle\langle\lambda(E)\rangle\rangle = \lambda_0(E/k_B T)^r$ r is 0 since we assumed that phonon scattering is dominant.

Material	λ_0	κ_l
Ge CB/VB	29/9.5	58
GaAs CB/VB	110/39	55
Bi_2Te_3 CB/VB	18/4	1.5

needed: (1) m^*_{DOM} for $M(E)$ calculation, (2) m^*_{DOS} obtain the reduced Fermi-level [$\eta_F = (E_F - E_C)/k_B T$] from measured carrier concentration. In the EMA,

$$S_{3D} = -\frac{k_B}{q}\left(\frac{(r+2)\cdot\mathfrak{F}_{r+1}(\eta_F)}{\mathfrak{F}_r(\eta_F)} - \eta_F\right), \tag{19}$$

$$G_{3D} = \lambda_0 \frac{2q^2}{h}\frac{m^*_{DOM}k_B T}{2\pi\hbar^2}\Gamma(r+2)\mathfrak{F}_r(\eta_F), \tag{20}$$

$$K_{e,3D} = \lambda_0 T\left(\frac{k_B}{q}\right)^2\frac{2q^2}{h}\frac{m^*_{DOM}k_B T}{2\pi\hbar^2}\Gamma(r+3)\left((r+3)\mathfrak{F}_{r+2}(\eta_F)\right.$$
$$\left. - \frac{(r+2)\mathfrak{F}^2_{r+1}(\eta_F)}{\mathfrak{F}_r(\eta_F)}\right), \tag{21}$$

where $\Gamma(j)$ is the Gamma function, the Fermi–Dirac integral of order j is defined as $\mathfrak{F}_j(\eta_F) = 1/\Gamma(j+1)\times\int_0^\infty dx\, x^j/(1+e^{x-\eta_F})$,[72] r is the characteristic exponent describing a specific scattering mechanism, and the parameter λ_0 is determined by comparison with experiments. Figures 5 and 7 show that effective mass theory provides a good agreement with full band atomistic simulation results.
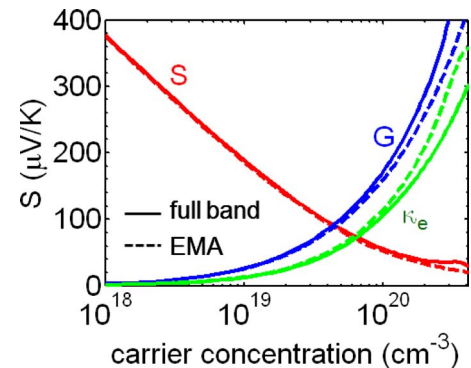

FIG. 7. (Color online) Comparison of EMA with full-band calculation for Ge. On the *y* axis, Seebeck coefficient (*S*), electrical conductivity (*G*) and thermal conductivity by electron (κ_e) are plotted from 0 to 400 μV/K, 0 to 4×10^6 Ω^{-1} m^{-1}, and 0 to 40 W m^{-1} K^{-1}.

Because the VBs are coupled and warped, it is difficult to predict m^*_{DOM} from the values of the heavy- and light-hole effective masses. Indeed, Table I shows a large discrepancy

$$E(k) - E_V = \frac{\hbar^2}{2m_x}\left[\gamma_1 k^2 \pm \sqrt{4\gamma_2^2 k^4 + 12(\gamma_3^2 - \gamma_2^2)(k_x^2 k_y^2 + k_y^2 k_z^2 + k_x^2 k_z^2)}\right] = Ak^2 \pm \sqrt{B^2 k^4 + C^2(k_x^2 k_y^2 + k_y^2 k_z^2 + k_x^2 k_z^2)}, \quad (22)$$

where γ_i are the Luttinger parameters and A, B, and C are constants.

From the definition of DOM, Eq. (11), it is hard to derive analytically the $M(E)$ versus E relation and then find analytical expression for m^*_{DOM}. But based on the counting bands approach, we can readily see why the extracted m^*_{DOM} is about two times larger than expected one from EMA.

Figure 8(a) shows that the CB of GaAs is nearly parabolic near the Γ point. According to the counting bands approach, e.g., Eq. (16), each band gives one conducting mode for electrons at a specific energy, E, due to parabolic behavior of dispersion relation. In other words, effective mass approximation assumes that each band gives one conducting channel for an injected electron having a specific wave vectors and energy E. When the bands are nearly parabolic, the analytic m^*_{DOM} agrees well with the m^*_{DOM} extracted from full band calculation, as we can see for the CB in Table I.

If we assume parabolic bands for the VB (heavy- and light hole) close to the Γ point, the m^*_{DOM} is expressed as $m^*_{\mathrm{DOM}} = m_{\mathrm{lh}} + m_{\mathrm{hh}}$, which is approximately two times less than the value extracted from full band calculation as shown in Table I. As clearly shown in the Fig. 8(b), most of bands for holes (especially for heavy-hole) contribute at least two conducting channels at a specific energy. The parabolic band assumption, however, gives one conducting channel per band and significantly underestimates the DOM for holes. Warped VBs provide more conducting modes.

Using this argument, we may also explain qualitatively the question of why m^*_{DOM} is different between Ge and GaAs even though the VBs look similar. Including results for Si and InAs VBs, the hole DOM effective mass, m^*_{DOM} extracted from full band calculations for Si, Ge, GaAs, and InAs are given as, $2.40m_0 > 1.63m_0 > 0.97m_0 > 0.65m_0$, re-

between the expected and numerically extracted values. From the Luttinger–Kohn model, the VB near the Γ point can be expressed as[73]

spectively. In Eq. (22), the degree of warping can be judged from the values of $(\gamma_3^2 - \gamma_2^2)/\gamma_2^2$, which we call the warping parameter. For $\gamma_3 = \gamma_2$, Eq. (22) yields two parabolic bands (heavy- and light- hole). From the tabulated values of γ_i,[73] the calculated warping parameter are $17 > 0.76 > 0.62 > 0.20$ for Si, Ge, GaAs, and InAs, respectively. This shows that the degree of warping can qualitatively explain the relative magnitude of m^*_{DOM} for Si, Ge, GaAs, and InAs even though the VB for all those diamondlike materials looks similar. One thing to note is that six-valley VB structure of Bi_2Te_3 is another reason for its high m^*_{DOM}.

V. SUMMARY AND CONCLUSION

The relation between the so-called transport distribution, which determines the TE coefficients and begins with the BTE, and the transmission obtained from the Landauer approach has been clarified in this paper. In particular, we showed how the mean-free-path for backscattering in the Landauer approach should be defined so that the Landauer approach is consistent with the BTE in the relaxation time approximation. We also showed that the transmission (transport distribution) is readily obtained from the full band description of the electronic bandstructure of a semiconductor using well-developed techniques—a simple semiclassical band counting method and a quantum mechanical approach. Several example calculations of the transmission and the TE coefficients for representative bulk materials were presented to demonstrate that Landauer approach provides an accurate description of experimentally measured TE parameters, In practice, the use of a constant mean-free-path in the Landauer approach is easier to justify than the use of a constant relaxation time in the Boltzmann equation. The Landauer approach also provides complementary insight into TE physics and can be applied to ballistic, quasiballistic, and quantum engineered structures. Finally, we showed that an accurate and simple effective mass model can be defined by extracting a DOM effective mass from the given full band results. One first computes $M(E)$ from Eq. (16) and then fits the linear portion near the band edge to Eq. (14). For accurate results, the fitting should be performed from the band edge to $\approx 5k_B T$ above the maximum expected Fermi level at the highest temperature of operation.
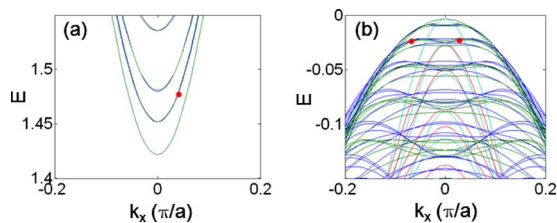

FIG. 8. (Color online) (Color online) Energy dispersion relation showing the lowest (a) CBs and (b) VBs of GaAs. (y axis ranges from EC (or EV) to EC (or EV) +5$k_B T$ because $-\partial f_0/\partial E$ spread about 5$k_B T$.) Each dot represents a conducting channels for positive moving electrons at specific energy for an electron moving with a positive velocity. In the VBs, most of the bands (especially heavy holes) have at least two conducting channels per energy

[1] M. Christensen, A. B. Abrahamsen, N. B. Christensen, F. Juranyi, N. H. Andersen, K. Lefmann, J. Andreasson, C. R. H. Bahl, and B. B. Iversen, Nature Mater. **7**, 811 (2008).

[2] L. D. Hicks, T. C. Harman, X. Sun, and M. S. Dresselhaus, Phys. Rev. B **53**, R10493 (1996).

[3] S. Woochul, K. Singer, A. Majumdar, J. Zide, A. Gossard, and A. Shakouri, in Proceedings of the 24th International Conference on Thermoelectrics (2005), pp. 9–12.

[4] W. Kim, S. L. Singer, A. Majumdar, D. Vashaee, Z. Bian, A. Shakouri, G. Zeng, J. E. Bowers, J. M. O. Zide, and A. C. Gossard, Appl. Phys. Lett. **88**, 242107 (2006).

[5] A. I. Hochbaum, R. Chen, R. D. Delgado, W. Liang, E. C. Garnett, M. Najarian, A. Majumdar, and P. Yang, Nature (London) **451**, 163 (2008).

[6] X. Sun, S. B. Cronin, J. Liu, K. L. Wang, T. Koga, M. S. Dresselhaus, and G. Chen, in Proceedings of the 18th International Conference on Thermoelectrics (1999), pp. 652–655.

[7] G. Joshi, H. Lee, Y. Lan, X. Wang, G. Zhu, D. Wang, R. W. Gould, D. C. Cuff, M. Y. Tang, M. S. Dresselhaus, G. Chen, and Z. Ren, Nano Lett. **8**, 4670 (2008).

[8] R. Venkatasubramanian, E. Siivola, T. Colpitts, and B. O'Quinn, Nature (London) **413**, 597 (2001).

[9] J. P. Heremans, V. Jovovic, E. S. Toberer, A. Saramat, K. Kurosaki, A. Charoenphakdee, S. Yamanaka, and G. Jeffrey Snyder, Science **321**, 554 (2008).

[10] T. Koga, X. Sun, S. B. Cronin, and M. S. Dresselhaus, Appl. Phys. Lett. **73**, 2950 (1998).

[11] T. Koga, S. B. Cronin, M. S. Dresselhaus, J. L. Liu, and K. L. Wang, Appl. Phys. Lett. **77**, 1490 (2000).

[12] D. J. Singh, *Materials Research Society Symposium Proceedings* (Materials Research Society, Warrendale, 2002), pp. 15–22.

[13] K. F. Hsu, S. Loo, F. Guo, W. Chen, J. S. Dyck, C. Uher, T. Hogan, E. K. Polychroniadis, and M. G. Kanatzidis, Science **303**, 818 (2004).

[14] S. Ohta, T. Nomura, H. Ohta, M. Hirano, H. Hosono, and K. Koumoto, Appl. Phys. Lett. **87**, 092108 (2005).

[15] G. J. Synder and E. S. Toberer, Nature Mater. **7**, 105 (2008).

[16] L. D. Hicks and M. S. Dresselhaus, Phys. Rev. B **47**, 16631 (1993).

[17] D. A. Broido and T. L. Reinecke, Appl. Phys. Lett. **67**, 100 (1995).

[18] O. Rabina, Y.-M. Lin, and M. S. Dresselhaus, Appl. Phys. Lett. **79**, 81 (2001).

[19] P. Martin, Z. Aksamija, E. Pop, and U. Ravaioli, Phys. Rev. Lett. **102**, 125503 (2009).

[20] T. Markussen, A.-P. Jauho, and M. Brandbyge, Phys. Rev. B **79**, 035415 (2009).

[21] N. Mingo, Appl. Phys. Lett. **84**, 2652 (2004).

[22] M. P. Singh and C. M. Bhandari, Solid State Commun. **127**, 649 (2003).

[23] E. B. Ramayya, D. Vasileska, S. M. Goodnick, and I. Knezevic, in Proceedings of the 8th IEEE Conference on Nanotechnology (2008), pp. 339–342.

[24] I. Bejenari and V. Kantser, Phys. Rev. B **78**, 115322 (2008).

[25] Y.-M. Lin, X. Sun, and M. S. Dresselhaus, Phys. Rev. B **62**, 4610 (2000).

[26] T. T. M. Vo, A. J. Williamson, V. Lordi, and G. Galli, Nano Lett. **8**, 1111 (2008).

[27] L. D. Hicks and M. S. Dresselhaus, Phys. Rev. B **47**, 12727 (1993).

[28] L. D. Hicks, T. C. Harman, and M. S. Dresselhaus, Appl. Phys. Lett. **63**, 3230 (1993).

[29] T. Koga, X. Sun, S. B. Cronin, and M. S. Dresselhaus, Appl. Phys. Lett. **75**, 2438 (1999).

[30] J. M. O. Zide, D. Vashaee, Z. X. Bian, G. Zeng, J. E. Bowers, A. Shakouri, and A. C. Gossard, Phys. Rev. B **74**, 205335 (2006).

[31] G. Wang and T. Cagin, Phys. Rev. B **76**, 075201 (2007).

[32] V. Rawat, Y. K. Koh, D. G. Cahill, and T. D. Sands, J. Appl. Phys. **105**, 024909 (2009).

[33] D. Vashaee and A. Shakouri, Phys. Rev. Lett. **92**, 106103 (2004).

[34] I. Chowdhury, R. Prasher, K. Lofgreen, G. Chrysler, S. Narasimhan, R. Mahajan, D. Koester, R. Alley, and R. Venkatasubramanian, Nat. Nanotechnol. **4**, 235 (2009).

[35] T. C. Harman, P. J. Taylor, M. P. Walsh, and B. E. LaForge, Science **297**, 2229 (2002).

[36] J. O. Sofo and G. D. Mahan, Appl. Phys. Lett. **65**, 2690 (1994).

[37] X. B. Zhao, X. H. Ji, Y. H. Zhang, T. J. Zhu, J. P. Tu, and X. B. Zhang, Appl. Phys. Lett. **86**, 062111 (2005).

[38] M.-S. Jeng, R. Yang, and G. Chen, in Proceedings of the 24th International Conference on Thermoelectrics (2005), pp. 21–26.

[39] H. Lee, D. Wang, W. Wang, and Z. Ren, B. Klotz, M. Y. Tang, R. Yang, P. Gogna, J.-P. Fleuiral, M. S. Dresselhaus, and G. Chen, in Proceedings of the 24th International Conference on Thermoelectrics (2005), pp. 269–271.

[40] T. Thonhauser, T. J. Scheidemantel, J. O. Sofo, J. V. Badding, and G. D. Mahan, Phys. Rev. B **68**, 085201 (2003).

[41] T. Borca-Tasciuc, W. Liu, J. Liu, T. Zeng, D. W. Song, C. D. Moore, G. Chen, K. L. Wang, M. S. Goorsky, and T. Radetic, Superlattices Microstruct. **28**, 199 (2000).

[42] D. A. Polvani, J. F. Meng, N. V. Chandra Shekar, J. Sharp, and J. V. Badding, Chem. Mater. **13**, 2068 (2001).

[43] G. D. Mahan and J. O. Sofo, *The Best Thermoelectric* (National Academy of Sciences, Washington, DC, 1996), pp. 7436–7439.

[44] R. Landauer, IBM J. Res. Dev. **1**, 223 (1957).

[45] S. Datta, *Electronic Transport in Mesoscopic Systems* (Cambridge University Press, New York, 1997), p. 393.

[46] R. Kim, S. Datta, and M. S. Lundstrom, J. Appl. Phys. **105**, 034506 (2009).

[47] P. Pecheur and G. Toussaint, Phys. Lett. A **135**, 223 (1989).

[48] S. Lee and P. von Allmen, Appl. Phys. Lett. **88**, 022107 (2006).

[49] T. J. Scheidemantel, C. Ambrosch-Draxl, T. Thonhauser, J. V. Badding, and J. O. Sofo, Phys. Rev. B **68**, 125210 (2003).

[50] K. Shin-ichi, J. Phys. Soc. Jpn. **26**, 58 (1969).

[51] P. M. Lee and L. Pincherle, Proc. Phys. Soc. (London) **81**, 461 (1963).

[52] S. K. Mishra, S. Satpathy, and O. Jepsen, J. Phys.: Condens. Matter **9**, 461 (1997).

[53] S. J. Youn and A. J. Freeman, Phys. Rev. B **63**, 085112 (2001).

[54] A. J. Miyoung, K. Freeman, and C. B. Geller, Phys. Rev. B **72**, 035205 (2005).

[55] B.-L. Huang and M. Kaviany, Phys. Rev. B **77**, 125209 (2008).

[56] I. I. Seong-Gon, K. Mazin, and D. J. Singh, Phys. Rev. B **57**, 6199 (1998).

[57] U. Sivan and Y. Imry, Phys. Rev. B **33**, 551 (1986).

[58] C. R. Proetto, Phys. Rev. B **44**, 9096 (1991).

[59] S. Datta, *Quantum Transport* (Cambridge University Press, New York, 2005), p. 404.

[60] E. O. Kane, J. Phys. Chem. Solids **1**, 249 (1957).

[61] E. C. E. Supriyo Datta, 495N Lecture 26: Ballistic Conductance (http://nanohub.org/resources/5725, 2008).

[62] N. Mingo, Phys. Rev. B **68**, 113308 (2003).

[63] C. Jeong, Calculating Number of Modes from Given E-K Dispersion (http://nanohub.org/resources/7382, 2009).

[64] M. Luisier, A. Schenk, W. Fichtner, and G. Klimeck, Phys. Rev. B **74**, 205323 (2006).

[65] J. M. Jancu, F. Bassani, F. Della Sala, and R. Scholz, Appl. Phys. Lett. **81**, 4838 (2002).

[66] G. Klimeck, F. Oyafuso, T. B. Boykin, R. C. Bowen, and P. von Allmen, Comput. Model. Eng. Sci. **3**, 601 (2002).

[67] T. B. Boykin, G. Klimeck, and F. Oyafuso, Phys. Rev. B **69**, 115201 (2004).

[68] P. Vogl, H. P. Hjalmarson, and J. D. Dow, J. Phys. Chem. Solids **44**, 365 (1983).

[69] H. J. Goldsmid, *Thermoelectric Refrigeration* (Plenum, New York, 1964).

[70] A. F. Ioffe, *Semiconductor Thermoelements and Thermoelectric Cooling* (Infosearch Limitied, 1957).

[71] P. B. Allen, W. E. Pickett, and H. Krakauer, Phys. Rev. B **37**, 7482 (1988).

[72] Raseong Kim and Mark Lundstrom, Notes on Fermi-Dirac Integrals (3rd Edition) (http://nanohub.org/resources/5475, 2008).

[73] K. W. Böer, *Survey of Semiconductor Physics: Electrons and Other Particles in Semiconductors* (Wiley, New York, 2002), p. 1291.

[74] J. S. Blakemore, J. Appl. Phys. **53**, R123 (1982).

[75] E. G. S. Paige, *The Electrical Conductivity of Germanium* (Heywood, London, 1964), p. 244.